Chalcogenide Letters Vol. 20, No. 10, October 2023, p. 697 - 708

Thermal conductivity and lattice dynamics of thermoelectric oxychalcogenide BiCuTeO

M. Guenfoud*, M. Hamouda
LDDI–Laboratory, Faculty of Science and Technology, University Ahmed Draia of Adrar,01000, Algeria

Recently, BiCuTeO is considered as one of the promising thermoelectric materials due to its ultra-low thermal conductivity. For this reason, the thermoelectric characteristic of this material has been studied to evaluate the lattice thermal conductivity (κ_L) from first-principles calculations which are based on solving linearized Boltzmann transport equations (LBTE) through the relaxation time (RTA) approximation. These calculations are used to predict the behavior of phonons in order to understand the origin of the ultra-low thermal conductivity of BiCuTeO. The lattice thermal conductivity of BiCuTeO is reproduced with high accuracy. Our calculations predict that BiCuTeO announces a strong anharmonicity, which is the cause of the very low value of the thermal conductivity. This results in very high group speeds. Moreover, the calculations of the elastic properties, dielectric constants, phonon group velocities, lifetimes, and Grüneisen parameters shows that the lattice thermal conductivity exhibits an obvious anisotropy.

(Received July 18, 2023; Accepted October 2, 2023)

Keywords: BiCuTeO, Thermal conductivity, Vibrational properties, Mechanical properties, Grüneisen parameters

1. Introduction

The thermal conductivity (κ_L) in materials is closely related to the vibration behavior of the crystal lattice, i.e., phonons. Therefore, knowledge of the contribution of phonons through their dispersion relations and their anharmonic effects, provides essential information on heat transport in order to design thermoelectric materials with low thermal conductivity. The Copper-bismuth Oxychalcogenide, formulated as BiCuXO (X = Te, Se) have become key materials for the production of thermoelectric energy from waste heat, due to their remarkable thermoelectric performances: excellent electronic transport and ultra-low thermal conductivity [1]. Among this group of materials, BiCuTeO Oxychalcogenide is recently involved in several thermoelectric (TE) applications due to the high value (TE) due to the high value (~0.42 at 373 K) of its figure of merit given as $ZT = S^2\sigma T/\kappa$, where S, σ, κ, and T are Seebeck coefficient, electrical conductivity, thermal conductivity, and absolute temperature, respectively [2], giving it remarkable thermoelectric performance. In addition, low thermal conductivity, the origin of which remains unclear. In order to explain the cause of this low conductivity. Recently, several first-principal studies have been conducted. Previous studies conducted by the experiment proposed that the low thermal conduction is due to the presence of the bi^{3+} lone pair, which may cause the lattice thermal conductivity to decrease due to the bond anharmonicity [3]. Pei *et al* [4] proposed that weak chemical bonding and strong anharmonicity lead to low thermal conductivity. Lin *et al*. [5] experimentally investigated thermal conductivity in BiCuTeO using Raman spectroscopy and inelastic neutron scattering. The generalized density of states of phonons (PDOS) revealed low values of average velocities of acoustic phonons compared to the majority of materials. In this work, we show an in-depth study of the phonon transport mechanisms for BiCuOTe with the aim of understanding the physical origin of the very low thermal conductivity as well as the very strong anisotropic character of phonon transport. The results of the calculations presented in this manuscript suggests that the optical phonons of BiCuTeO contribute significantly to the

* Corresponding author: sciencestech@yahoo.fr
https://doi.org/10.15251/CL.2023.2010.697

conductivity and show that the obvious anisotropy of phonon conduction comes from the anisotropic sound velocities in BiCuTeO. The rest of the paper is processed as follows. The calculation method is introduced and described in the second section. In the third section, the main results are presented and discussed. Finally, a summary of our main results is presented at the end of this article.

2. Computational methods

The DFT calculations in the present work were performed by the VASP code [6–9]. Exchange and correlation effects have been treated in the GGA-PBE approximation, using the Perdew, Burke and Ernzernhof functional (PBE) [10]. O: $2s^2 2p^4$, the Cu: $4s^1 4d^{10}$, the Bi: $6s^2 6p^3$ and the Te: $5s^2 5p^4$ are respectively treated as electronic valence states. The plane wave energy cutoff was set at 560 eV, and the Brillouin zone was sampled on 8×8×8 k-point grid. The total energy convergence is 10^{-8} eV/atom, and the atomic relaxation was stopped when the Hellmann-Feynaman ionic strengths fell below 10^{-3} eV/Å. The Calculations of the vibrational characteristics of phonons were performed within the framework of density functional perturbation theory (DFPT), as implemented in the code phonopy [11,12]. Born's effective charges were calculated taking into account long-range electrostatic forces. The second and third order force constants were obtained by the supercell approach [13,14] with a finite atomic displacement of 0.03 Å. In this process, a 3×3×2 supercell containing 144 atoms is used for harmonic and anharmonic IFC calculations, respectively. For sampling the Brillouin zone, the reciprocal cells of the supercells were sampled with a 2 × 2 × 2 k-point mesh using the Monkhorst-Pack scheme [14].

3. Results and discussion

3.1. Structural and mechanical properties

CuBiTeO crystallize in a tetragonal structure with a space group P4/nmm [15], as shown in Fig. 1. The primitive cell of BiCuTeO contains eight atoms, occupying the following positions: O: 2a (0.75, 0.25, 0), Cu: 2b (0.75, 0.25, 0.5), Bi: 2c (0.25, 0.25, z (Bi)), and Te: 2c (0.25, 0.25, z (Te)).

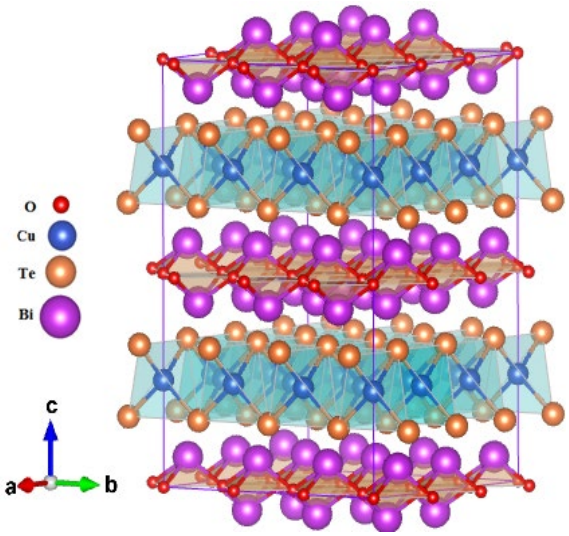

Fig. 1. Crystal structure of BiCuTeO.

The structural parameters are acquired by calculating the total energy as a function of the unit cell volumes around the equilibrium volume V_0. The (V_i, E_i) results are fitted to the Birch-

Murnaghan equation of state EOS [16]. The calculated equilibrium crystal-structure parameters *a* (c) (in unit Å) and Born effective charges at room temperature for BiCuTeO is presented in table 1. The optimized lattice constants (a and c) are in excellent agreement with experiment [17], with typical deviations of < 1%.

Table 1. Calculated equilibrium lattice constants (a and c in Å), Born effective charges $z_{M,\alpha}$, and dielectric constants $\varepsilon_{\infty,\alpha}$ of BiCuTeO.

Method	*a (Å)*	*c (Å)*	*zBi∥*	*zB⊥*	*zCu∥*	*zCu⊥*	*zO∥*	*zO⊥*	*zTe∥*	*zTe⊥*	*ε∞∥*	*ε∞⊥*
This work	4.05	9.50	6.47	6.44	0.86	1.23	−4.61	−4.98	−2.68	−2.71	15.75	17.05
Ref. [18]	3.99	9.51	6.50	6.38	0.97	1.24	−4.44	−4.89	−2.59	−2.73	15.80	17.11
Exp. [17]	4.04	9.52	–	–	–	–	–	–	–	–	–	–

Born effective charges (BCE) and calculated dielectric constants of BiCuTeO are listed in Table 2. Our calculations of Born effective charges (BCE) and dielectric constants are in good agreement with the calculations of Hyo Seok Ji [18]. The Born effective charges (BCE) and dielectric constants provide important information about the bond type and the distribution of optical phonons in the phonon dispersion relationship. Our results indicate a significant difference between the values of (BCE) Z_{xx} and Z_{zz} leading to considerable anisotropy. It should also be noted that the very high values of the Born effective charges (BCE) for Bi and O (see Table 2) suggests that the covalent nature of the (Bi-O) bond is predominant over the (Cu-Te) bond [19]. The high dielectric constants ($\varepsilon_{\infty,\|}$ = 15.80 and $\varepsilon_{\infty,\perp}$ = 17.11) also indicate a strong presence of acoustic phonons in the dispersion relation, which is consistent with the presence of heavy atoms (Bi and Te) in the BiCuOTe crystal.The elastic properties give important information about many fundamental properties, such as speed of sound, Debye temperature, thermal conductivity as well as anisotropy. Owing to the symmetry of tetragonal structure, BiCuTeO compound have six independent components of elastic constants, namely: C_{11}, C_{12}, C_{13}, C_{33}, C_{44} and C_{66}, respectively. The calculated values of the elastic constants were checked by Born elastic stability criteria [20], which for the tetragonal crystals are: $C_{11} > 0$, $C_{33} > 0$, $C_{44} > 0$, $C_{66} > 0$, $C_{11} > |C_{12}|$, $C_{11}C_{33} > C^2_{13}$ and $2C^2_{13} < C_{33}(C_{11} + C_{12})$. The elastic constants C_{ij} obtained are presented in table 2. We find that the C_{ij} of the BiCuTeO are all positive and satisfy these mechanical stability criteria. This affirms that the BiCuTeO is mechanically stable.

\

Table 2. Calculated lattice properties of the BiCuTeQ compounds: elastic constants Cij, bulk (B), shear (G), and Young (E) moduli (in GPa). Available experimental results [18].

Refs.	C_{11}	C_{12}	C_{13}	C_{33}	C_{44}	C_{66}	*B*	*G*	*E*
Present work	146.8	57.8	58.9	100.4	38.4	22.2	81.5	29.8	79.7
Réf. [18]	143.9	57.2	58.3	98.8	37.8	22.5	80.3	34.7	91.1

In addition, C_{33} has a smaller value than C_{11}, which means BiCuTeO is easily compressed along the c-axis with respect to the *a*-axis. With the elastic constants found, the bulk (*B*) and shear (*G*), were estimated by using the Voigt–Reuss–Hill average [21–24]. The Young modulus (*E*) is related to *B* and *G* [25–26] as

$$E = \frac{9BG}{3B + G} \quad (1)$$

The calculated bulk modulus *B* of the BiCuTeO is 81.5 GPa, which is in agreement with the result of 77.20 GPa obtained from fitting Birch-Murnaghan (EOS). Moreover, the ratio of bulk modulus *B* along *a* axis to that along the axis c can be deduced by [27]

$$\frac{B_a}{B_c} = \frac{(c_{22}-c_{12})(c_{11}-c_{13})-(c_{11}-c_{12})(c_{23}-c_{12})}{(c_{22}-c_{12})(c_{33}-c_{13})-(c_{12}-c_{23})(c_{13}-c_{23})} \quad (2)$$

The high value of the *Ba*/*Bc* ratio = 2.5 for BiCuOTe implies a strong anisotropy. This value is very close to the ratio of k_{xx} *to* k_{zz} (see Fig. 3). Therefore, our calculations show that the strong lattice thermal conductivity anisotropy in BiCuOTe should be attributed to the bulk modulus anisotropy, which causes anisotropic velocities in BiCuOTe.

3.2. Vibrational properties

Figure 2 show the phonon dispersion and phonon DOS of the BiCuTeO. All phonon frequencies in the dispersion curve are positive along the Brillouin zone, implying that the structure of BiCuTeO is mechanically stable. The low frequency acoustic modes are separated from the high frequency optical modes by a difference of 1 THz. Note that near the point Γ, strong corrections are provided to the phonon modes by the non-analytical term (LO-TO). Therefore, the phonon spectrum does not appear continuous at the point Γ. We can distinguish relatively two regions at the point Γ: The low frequency zone around 0-5 THz, the vibrations of the O atoms are completely decoupled and the vibration of the low frequency acoustic and optical modes comes mainly from the vibrations of Bi, Cu atoms and Te, and the high frequency region above 7 THz, comes mainly from the vibration of the O atom due to its light atomic mass, implying that these modes exhibit obvious dispersion, indicating that they have relatively group velocities important. An important point to emphasize is that the optical modes (high frequencies) have an obvious dispersion, indicating that their group velocities must be higher than those of the acoustic modes and the optical modes (low frequencies Moreover, the dispersions of the acoustic branches and of certain optical branches along the plane (Γ–Z) and different from those of the (Γ–X) plane, implying strong phonon anisotropy.

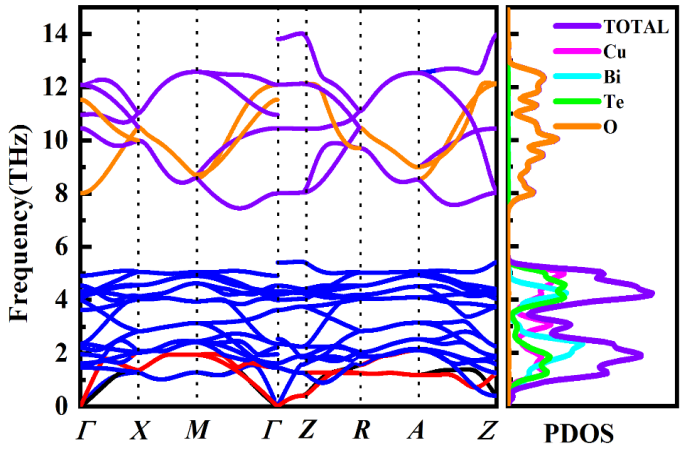

Fig. 2. Phonon dispersion and the phonon DOS of BiCuTeO.

3.3. Thermal Transport Properties

3.3.1. Lattice thermal conductivity

The lattice thermal conductivity of phonons can be calculated within the single-mode relaxation time (RTA) approximation which is implemented in the PHONO3PY package [28]. The macroscopic thermal conductivity tensor κ_L is defined as the sum of the individual phonon mode contributions λ according to [29]

$$\boldsymbol{\kappa}_L = \frac{1}{NV_0}\sum_{\lambda} \boldsymbol{\kappa}_{\lambda} = \frac{1}{NV_0}\sum_{\lambda} C_{\lambda}\, \mathrm{v}_{\lambda} \otimes \mathrm{v}_{\lambda}\tau_{\lambda} \qquad (3)$$

where $\boldsymbol{\kappa}_{\lambda}$ are the modal thermal conductivities, C_{λ} is the modal heat capacity, V_0 is the volume of a unit cell, N is the number of uniformly spaced q points in the Brillouin zone, and $\boldsymbol{\nu}_{\lambda}$ and τ_{λ} are the the group velocity and phonon lifetime for phonon mode λ. Figure 3 presents the variation of the lattice thermal conductivity as a function of temperature along *a* (κ_{xx}) and c (κ_{zz}) axis, and the average thermal conductivitie of BiCuOTe. The thermal conductivity of BiCuTeO decreases when the temperature increases, which could be assign to Umklapp scatterings of phonons [30,31]. Besides the thermal conductivity shows obvious anisotropy along the a and c directions, where the lattice thermal conductivity along a direction is much greater than that along the c direction. The average thermal conductivity is defined as [32]: $\kappa_{average} = (\kappa_{xx} + \kappa_{yy} + \kappa_{zz})/3$. As shown in Fig. 3, the $\kappa_{average}$ calculated at 300 K is 0.49 $Wm^{-1}K^{-1}$, which is in good agreement with the experimental results [33]. The lattice thermal conductivity of BiCuTeO at 300 K along the *a* (κ_{xx}) *and c* (κ_{zz}) axis is 0.642 W/m K and 0.191 W/m K, respectively. The inset of the figure shows the ratio of $k_{\_xx}$ *to* $k_{\_zz}$ which is 2.5 ~ 3.5, which implies strong anisotropy. This anisotropy is present over the entire temperature space of this study.

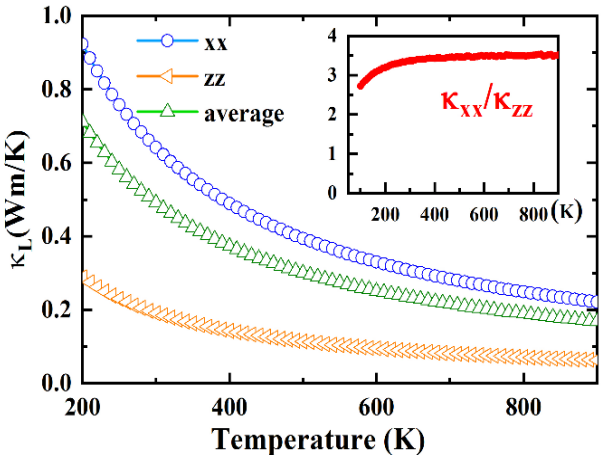

Fig. 3. Temperature-dependent κ_{xx}, κ_{zz} *and* $\kappa_{average}$ *of BiCuOTe. The inset of the figure shows the ratio of* κ_{xx} *to* κ_{zz}.

The lattice thermal conductivity anisotropy can be explained in two ways. the acoustic branches and part of optical branches have different dispersions according to the directions (Γ–X) and (Γ–Z), hence different group speeds along these directions. Very strong covalent and ionic bonding interactions along xx directions, and weak electrostatic interactions along zz directions are very different. Therefore, weak electrostatic interactions along the xx direction prevent the transport of phonons and therefore leads to a low thermal conductivity κ_L [34]. To better understand which phonon modes, contribute the most to the thermal conductivity, we calculated the accumulated lattice thermal conductivity κ_L along the axis a(xx), c(zz), and their average κ_{ave}, as a function of the frequency at the ambient temperature. The derivatives of the cumulative values of κ_{xx} and κ_{zz} are also illustrated in Figure 4.b. A first reading of the curves allows us to note that the thermal conductivity of BiCuTeO is anisotropic with larger values of κ_L along of the axis *a*(xx), compared to that of the axis c(zz), for the whole range of studied frequency. This observation is analogous to other previous theoretical work [35]. In addition, the cumulative thermal conductivities in the a and c directions continue to increase as the frequency increases, and gradually approach the plateau after the frequencies reach a maximum value around w=4 THz. In the high frequency region, the optical phonons of frequency between 7 and 11 THz, contribute strongly to κ_L, a feature that has already been pointed out in the manuscript. Moreover, the

derivatives of κ_L as a function of phonon frequencies provide information on the density of the carrier phonons according to their frequencies and their contribution to thermal conductivity. This phonon density vanishes in a frequency range from 4 THz to 7 THz, in which κ_L reaches a plateau. This region is almost identical to that which separates the acoustic modes and optical modes (see Figure 2). Note also that the contribution of these modes to the thermal conductivity in the x-plane is greater than that of the z-plane in the entire frequency range of our study. while in the optical phonon region, the contribution is only in the x-plane.

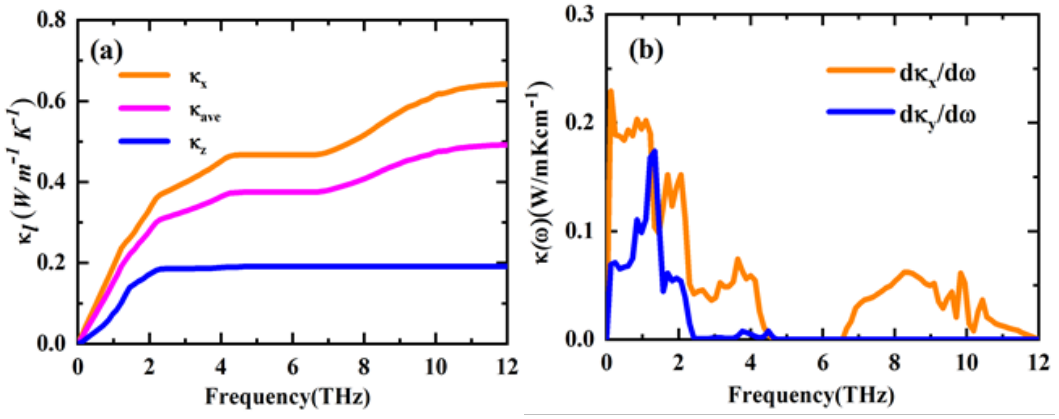

Fig. 4. a) Cumulative lattice thermal conductivity κ_L, and b) Derived from κ_{xx} and κ_{zz} versus frequencies for BiCuOTe at T = 300 K.

3.3.2. Phonon group velocities, lifetimes, and Grüneisen parameters

In order to explain the reason of the very low conductivity of the compound BiCuOTe, the phonon group velocities, the lifetime and the Grüneisen parameters have to be calculated and analyzed. For this, we start with the analysis of the anisotropy of phonon group velocities in BiCuOTe. The phonon velocities are closely related to the phonon transport of BiCuOTe. In general, low values of phonon velocities give low conductivity [5]. This is consistent with Figure 5, which shows the phonon group velocities as a function of frequency along the Γ–X and Γ–Z directions for BiCuTeO at 300 K. From figure 5, it is clear that the phonon group velocities optics are larger than that of acoustic phonons. Moreover, the phonon velocities in the plane (Γ–X) are different from those of the (Γ–Z) plane, which reveals a strong anisotropy of the thermal conductivity. Figure 5 also shows that the group velocities along the *a*-axis are greater than those along the c-axis, especially for high-frequency optical modes.

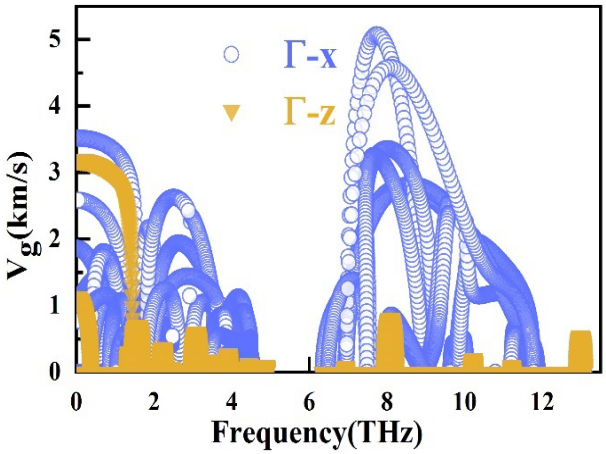

Fig. 5. Phonon group velocities as a function of frequency for BiCuTeO at 300 K.

The phonon lifetimes τ_λ is an essential parameter in determining the scattering rates of phonons in a solid. τ_λ are calculated as the inverse of the phonon linewidths Γ_λ as [36]

$$\tau_\lambda = \frac{1}{2\Gamma_\lambda} \tag{4}$$

The phonon Γ_λ can be determined from the sum of the three-phonons scattering processes [36]

$$\Gamma_\lambda = \frac{18\pi}{\hbar^2}\sum_{\lambda'\lambda''} |\Phi_{-\lambda\lambda''\lambda''}|^2 \times \{(n_{\lambda'} + n_{\lambda''} + 1)\delta(\omega_\lambda - \omega_{\lambda'} - \omega_{\lambda''}) + (n_{\lambda'} - n_{\lambda''})[\delta(\omega_\lambda + \omega_{\lambda'} - \omega_{\lambda''}) + \delta(\omega_\lambda - \omega_{\lambda'} + \omega_{\lambda''})]\} \tag{5}$$

where $\Phi_{\lambda\lambda'\lambda''}$ is the interaction force between the three phonons λ, λ', and λ'' participate in the diffusion and n_λ are the mode occupation numbers.

The phonon lifetimes of BiCuOTe at room temperature are shown in Fig. 6. According to this figure, the frequency dependence trends of the lifetimes show an ω^{-2} dependence in the low frequency regime as predicted by Klemens on the other hand the lifetimes of the optical modes above 7 THz have values different from those given by Klemens' relation [37,38].

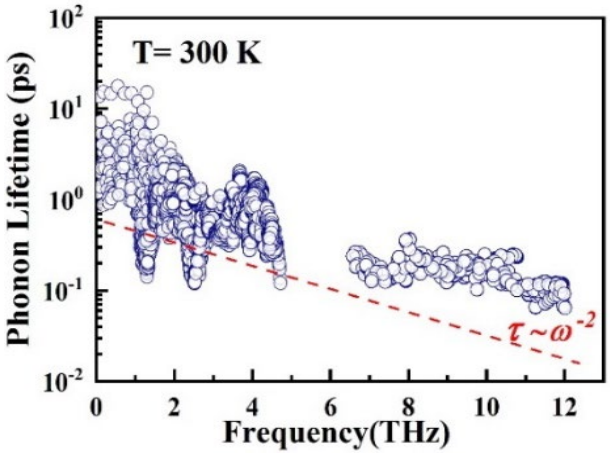

Fig. 6. Frequency-dependent phonon lifetimes of BiCuOTe at T=300 K.

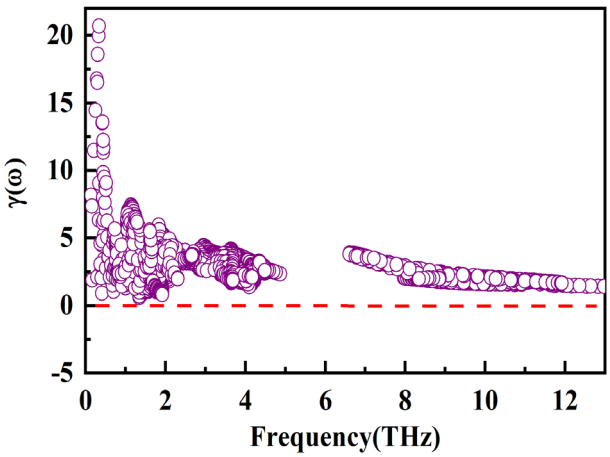

Fig. 7. Frequency-dependent mode Grüneisen parameters of BiCuOTe.

The Grüneisen parameters $\gamma_{(\lambda,q)}$can give good information on the anharmonic interactions of a crystal. In general, it can be deduced from the relation between phonon frequency and volume change as below [39–41]

$$\gamma_{(\lambda,q)} = \frac{-V}{\omega_{\lambda,q}} \frac{\partial \omega_{\lambda,q}}{\partial V} \tag{6}$$

Usually, a large value of | γ | means that it could have a strong phonon-phonon anharmonic scattering with too short a phonon relaxation time [42]. From figure 7, BiCuTeO has large | γ | values for phonon acoustic modes (~ −20) causing a strong interaction between phonons and thus leading to an abrupt decrease in thermal conductivity in BiCuTeO. According to Slack's theory [43–45], the long phonon lifetimes, low phonon velocities, and high phonon anharmonicity will result in ultralow thermal conductivity in BiCuOTe.

3.3.3. The joint density of state (JDOS), phonon linewidth and the mean phonon free path

In order to be able to further study the process of three phonon scattering, we determine the joint density of state (JDOS) which is given by the following formula [32]

$$Q_{\pm}(\omega) = \sum_{p_1 p' p''} \delta\left(\omega - \omega_p(\boldsymbol{q})\right) \iint_{\mathrm{BZ}} \delta\left(\omega_p(\boldsymbol{q}) \pm \omega'_p(\boldsymbol{q}') - \omega''_p(\boldsymbol{q} \pm \boldsymbol{q}' - G)\right) d\boldsymbol{q} d\boldsymbol{q}'. \tag{7}$$

where the ω_p, ω'_p, and ω''_p are the frequencies of the three-phonon scattering, Q+ corresponds to the absorption processes, and Q− is for the emission processes.

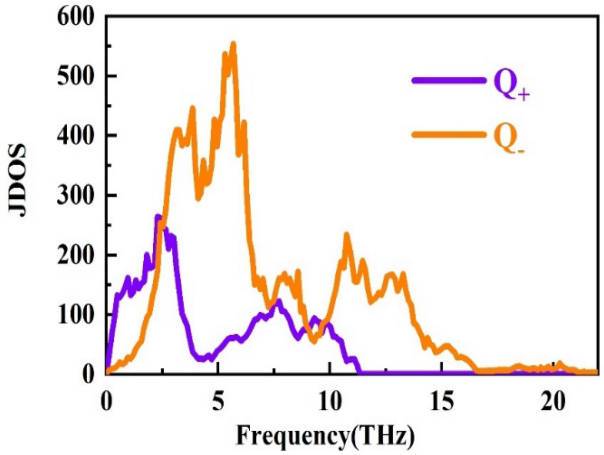

Fig. 8. The joint density of states (JDOS) for 3-phonon scattering as a function of frequency for BiCuTeO.

The analysis of the contributions of the different phonon branches in the phonon JDOS for BiCuTeO, suggests that low-frequency phonons (acoustic modes) contribute significantly to emission and absorption mechanisms compared to high-frequency phonons (optical modes). Additionally, the high frequency region above 7 THz mainly results from the vibration of the O atom because of its light atomic mass, which implies that these modes exhibit obvious dispersion, indicating that they have relatively large group velocities. Therefore, optical phonons contribute much more to the thermal conductivity in BiCuOTe. Figure 9 presents frequency dependence of a phonon linewidth and the mean phonon free path of BiCuTeO at 300 K. From Fig. 9a, we see that the scattering rates of high frequency optical phonons are clearly superior compared to acoustic phonons. Whereas at low frequencies (ω < 7 THz) the scattering rates of optical and acoustic phonons are comparable. The mean phonon free path (MFP) is a physical parameter essential to

determine the thermal properties of a material. Generally, it describes the transport behavior of phonons in a material. MFP is related to group velocities and relaxation time by the following formula [46–49]

$$|\Lambda_\lambda| = |v_\lambda| \times \tau_\lambda \tag{8}$$

The prediction of the mean free path of phonons Λ is an important means for the control of heat in materials at the nanometric scale of size comparable to Λ. If the scale of the system becomes smaller than Λ, the thermal conductivity will be significantly reduced due to phonon scattering [50]. Figure 9.b presents the variation of the mean free path (MFP) of BiCuTeO as a function of frequency. We show that at low frequencies where the acoustic modes are present, the MFPs reach maximum values of 10 nm. While for the optical modes, the maximum values of MFP do not exceed 1 nm. This leads to a strong participation of optical modes to the thermal conductivity of BiCuTeO films.

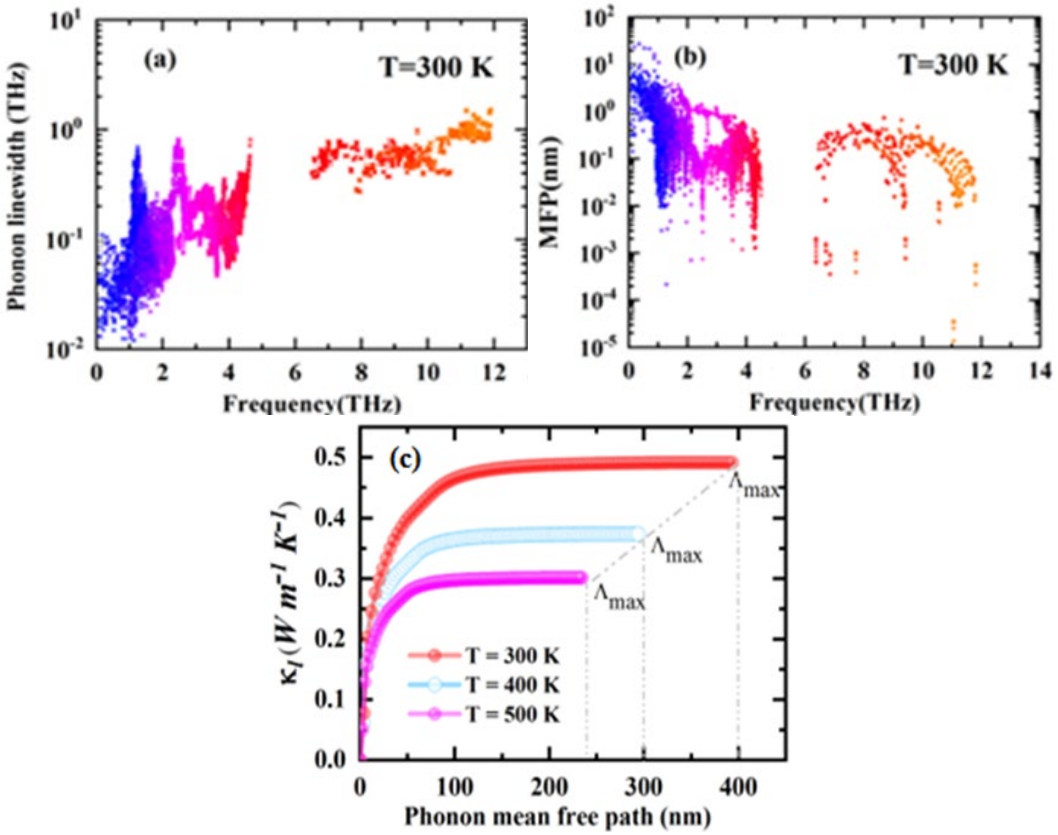

Fig. 9. Frequency dependence of: a) phonon linewidth, b) phonon MFP of BiCuTeO at 300 K, and c) Cumulative lattice thermal conductivity of BiCuTeO as a function of phonon mean free path at three different temperatures.

Figure 9.c shows average thermal conductivity κ_L of the BiCuTeO compound as a function of mean free path (MFP) for three different temperatures. We observe that κ_L continues to increase as the PMF increases and gradually approaches the plateau after the MFPs reach maximum values of Λ_{max} (T = 300 K, $\Lambda_{max} \sim 393$ nm; T = 400 K, $\Lambda_{max} \sim 294$ nm; T = 300 K, $\Lambda_{max} \sim 235$ nm), according to: $\Lambda \propto 1/T$. Moreover, at higher temperatures the contribution of phonons with shorter MFPs to the conductivity becomes important. Figure 9.c clearly shows that most of the heat is transported by vibrational modes with λ ranging from 1 to 100 nm at 300 K because when the temperature decreases, the mean free paths of the phonons increase and become larger than the size of the spot. Therefore, the quasi-ballistic thermal conduction effect appears and causes a

reduction in the conductivity [51]. Finally, figure 9.c can help enormously in the optimization of the grain size of the CuBiTeO crystal, in the spirit of reducing its conductivity and improve its thermoelectric performance.

4. Conclusions

In this manuscript, we have brought a detailed study on the transport of phonons and its effect on the thermal conductivity. First, the structural, mechanical and vibrational properties of BiCuTeO have been investigated with First-principles calculations and Boltzmann phonon transport theory. To explain the origin of the very low conductivity of the BiCuOTe compound, phonon lifetimes, the Grüneisen parameters and the phonon group velocities were calculated and analyzed. Our results show the presence of a strong anharmonicity of the phonon group velocities along the a and c axes, which is probably due to the chemical bond anisotropy of BiCuOTe. In addition, our first-principles calculations show that high-frequency phonons (optical modes) contribute much less to the scattering process and that their group velocities are relatively large. Therefore, the optical modes largely contribute to the conductivity in BiCuOTe. This work should offer new perspectives and a broad avenue for the study of phonon transport processes in various materials in order to obtain a good control of thermal conductivity at the nanometric scale.

Acknowledgments

We gratefully acknowledge computing support provided by the Research Center on Scientific & Technical Information (CERIST) in Algiers (Algeria) through the High-Performance Computing Platform (HPC) IBNBADIS.

References

[1] X. Yang, Z. Sun, G. Ge, J. Yang, Materials, 16(12),4318 (2023); https://doi.org/10.3390/ma16124318
[2] S. Muhammady, Y. Kurniawan, S. Ishiwata, A. Rousuli, T. Nagasaki, S. Nakamura, Inorganic Chemistry, 57(16), 10214 (2018); https://doi.org/10.1021/acs.inorgchem.8b01396
[3] P. Vaqueiro, R.A.R. Al Orabi, S. D.N. Luu, G. Guelou, A. V. Powell, Phys. Chem. Chem. Phys, 17(47), 31735 (2015); https://doi.org/10.1039/C5CP06192J
[4] Y. Pei, J. He, J. Li, F. Li, Q. Liu, W. Pan, C. Barreteau, NPG Asia Mater 5, e47 (2013); https://doi.org/10.1038/am.2013.15
[5] D. Lin, S. T. Dong, Y. Y. Zhang, Y. Y. Lv, J. Zhou, Y. B Chen, Journal of Alloys and Compounds, 826, 154161(2020); https://doi.org/10.1016/j.jallcom.2020.154161
[6] G. Kresse, J. Furthmuller, Phys. Rev. B 54, 11169 (1996); https://doi.org/10.1103/PhysRevB.54.11169
[7] G. Kresse, J. Furthmuller, Comput. Mater. Sci. 615, (1996); http://dx.doi.org/10.1016/0927-0256(96)00008-0
[8] G. Kresse, D/ Joubert, Phys. Rev. B 59, 1758 (1999); http://dx.doi.org/10.1103/PhysRevB.59.1758
[9] J. Hafner, Computer physics communications 177, 6 (2017) ; https://doi.org/10.1016/j.cpc.2007.02.045
[10] J. P. Perdew, K. Burke, M. Ernzerhof, Phys. Rev. Lett. 78, 1396 (1997); https://doi.org/10.1103/PhysRevLett.78.1396
[11] H. J. Monkhorst, J. D. Pack, Phys. Rev. B 13, 5188 (1976); https://doi.org/10.1103/PhysRevB.13.5188
[12] A. Togo, F. Oba, and I. Tanaka, Phys. Rev. B 78, 13410 (2008); https://doi.org/10.1103/PhysRevB.78.134106

[13] M. J. L. Angster, A. R. Q. Hussain, Physica B+ C, 131(1-3), 119(1985); https://doi.org/10.1016/0378-4363(85)90145-7
[14] M. Cruz, M. R Beltrכn, C. Wang, J. Tagüeٌa-Martىnez, Physical Review B, 59(23), 15381 (1999); https://doi.org/10.1103/PhysRevB.59.15381
[15] S. Tippireddy, P. K. DS, S. Das, R. C. Mallik, ACS Applied Energy Materials, 4(3), 2022 (2021); https://doi.org/10.1021/acsaem.0c02770
[16] F. Birch, Phys. Rev. 71, 809 (1947) https://doi.org/10.1103/PhysRev.71.809
[17] H. Hiramatsu, H. Yanagi, T. Kamiya, K. Ueda, M. Hirano, and H. Hosono, Chem. Mater. 20(1), 326 (2008); http://dx.doi.org/10.1021/cm702303r
[18] H. S. Ji, A. Togo, M. Kaviany, and I. Tanaka, Phys. Rev. B 94, 115203(2016); http://dx.doi.org/10.1103/PhysRevB.94.115203
[19] S. K. Saha, Phys. Rev. B, 92(4), 041202(2015); http://dx.doi.org/10.1103/PhysRevB.92.041202
[20] M. Born, K. Huang, Oxford: Clarendon (1954); https://doi.org/10.1119/1.1934059
[21] W. Voigt, Lehrbuch der Kristallphysik, Taubner, Leipzig, (1928);
[22] A. Reuss, Z. Angew, Math. Mech. 9, 49 (1929); https://doi.org/10.1002/zamm.19290090104
[23] R. Hill, Proc. Phys. Soc. A 65, 350 (1952); https://doi.org/10.1088/0370-1298/65/5/307
[24] G. Simmons, H. Wang, *A Handbook*. Second edition, MIT Press, Cambridge, MA, (1971);
[25] S. Tomar, R. Gautam, C. Negi, S. Gupta, S. Bhardwaj, A. Verma, Chalcogenide Letters. 16(1), 1 (2019); https://doi.org/10.15251/CL.2023.202.101
[26] M. Guenfoud, M. Hamouda, I. Arbaoui, Chalcogenide Letters, 18(9) (2021); https://doi.org/10.15251/CL.2021.189.493
[27] J. N. Yuan, Y. Cheng, X. Q. Zhang, X. R. Chen, L. C. Cai, *Zeitschrift für Naturforschung A*, *70*(7), 529-537 (2015); https://doi.org/10.1515/zna-2015-0102
[28] A. Togo, L. Chaput, T. Tadano, and I. Tanaka, Journal of Physics: Condensed Matter (2023); https://doi.org/10.1088/1361-648X/acd831
[29] A. Togo, L. Chaput, I. Tanaka, Phys. Rev. B 91, 094306 (2015); https://doi.org/10.1103/PhysRevB.91.094306
[30] Burchell, T. D. Encyclopedia of Materials: Science and Technology, 6310-6319, (2001); https://doi.org/10.1016/B0-08-043152-6/01120-7
[31] A. Balandin, K. L. Wang, Physical Review B, 58(3), 1544, https://doi.org/10.1103/PhysRevB.58.1544
[32] H. Shao, X. Tan, G. Q. Liu, J. Jiang, H. Jiang, Scientific Reports, 6(1), 21035 (2016); https://doi.org/10.1038/srep21035
[33] P. Vaqueiro, G. Guélou, M. Stec, E. Guilmeau, and A. V. Powell, J. Mater. Chem. A 1, 520 (2013); https://doi.org/10.1039/C2TA00878E
[34] J. Li, W. Zhai, C. Zhang, Y. Y.an, P. F. Liu, G. Yang, Materials Advances, 2(14), 4876(2021); https://doi.org/10.1039/D1MA00375E
[35] G. Liu, H. Sun, J. Zhou, Q. Li, X. G. Wan, Journal of Applied Physics, 119(18). (2016); https://doi.org/10.1063/1.4949485
[36] A. A. Maradudin and A. E. Fein, Phys. Rev. 128, 2589 (1962); https://doi.org/10.1103/PhysRev.128.2589
[37] P. G. Klemens, Physical review, 119(2), 507(1960); https://doi.org/10.1103/PhysRev.119.507
[38] P. G. Klemens, Solid state physics, Vol. 7. Academic Press, 1-98(1958); https://doi.org/10.1016/S0081-1947(08)60551-2
[39] K. Brugger. Physical Review, 137(6A), A1826 (1965); https://doi.org/10.1103/PhysRev.137.A1826
[40] N. L. Vočadlo, G. D. Price, Physics of the earth and planetary interiors, 82(3-4), 261(1994); https://doi.org/10.1016/0031-9201(94)90076-0
[41] A. C. Holt, M. Ross, Physical Review B, 1(6), 2700(1970); https://doi.org/10.1103/PhysRevB.1.2700

[42] X. Yan, B. Wang, Y. Hai, D. R. Kripalani, Science China Physics, Mechanics & Astronomy, 65(11), 117004(2022); https://doi.org/10.1007/s11433-022-1949-9
[43] G. A. Slack, Solid State Phys., 34, 1-71(1979); https://doi.org/10.1016/S0081-1947(08)60359-8
[44] Y. Zhang, C. Ling, Npj Computational Materials, 4(1), 25(2018); https://doi.org/10.1038/s41524-018-0081-z
[45] X. Shi, L. Chen, C. Uher, International Materials Reviews, 61(6), 379-415(2016); https://doi.org/10.1080/09506608.2016.1183075
[46] T. Luo, J. Garg, J. Shiomi, K. Esfarjani, G. Chen, Europhysics Letters, 101(1), 16001(2013); https://doi.org/10.1209/0295-5075/101/16001
[47] A. J. McGaughey, M. Kaviany, Physical Review B, 69(9), 094303. (2004); https://doi.org/10.1103/PhysRevB.69.094303
[48] A. Negi, A. Rodriguez, X. Zhang, A. H. Comstock, C. Yang, D. Sun, J. Liu, Advanced Science, 2301273 (2023); https://doi.org/10.1002/advs.202301273
[49] Z. Cheng, W. Lu, J. Shi, D. Tanaka, N. H. Protik, S. Wang, S. Graham, Materials Today Physics, 20, 100462(2021); https://doi.org/10.1016/j.mtphys.2021.10046
[50] Y. Hu, L. Zeng, A. J. Minnich, M. S. Dresselhaus, G. Chen, Nature nanotechnology, 10(8), 701-706 (2015); https://doi.org/10.1038/nnano.2015.109
[51] O. Bourgeois, D. Tainoff, A. Tavakoli, Y. Liu, C. Blanc, M. Boukhari, and E. Hadji, Comptes Rendus Physique, 17(10), 1154-1160 (2016); https://doi.org/10.1016/j.crhy.2016.08.008